Associated relationship between ventilation rates and indoor air quality

Article *in* RSC Advances · November 2016

DOI: 10.1039/C6RA22902F

3 authors, including:

Shi-Jie Cao
Southeast University (China)
61 PUBLICATIONS **715** CITATIONS

SEE PROFILE

RSC Advances

PAPER

View Article Online
View Journal | View Issue

Cite this: *RSC Adv.*, 2016, **6**, 111427

Associated relationship between ventilation rates and indoor air quality

Shi-Jie Cao,* Dong-Hao Zhu and Yin-Bao Yang

Received 13th September 2016
Accepted 5th November 2016

DOI: 10.1039/c6ra22902f

www.rsc.org/advances

Ventilation represents a significant portion of building energy consumption. Current codes and standards do not offer adequate guidance with respect to energy efficiency and to the relationship between the ventilation rate and the degree of indoor hazard. For the sake of energy savings, it is of great importance to study the associations between ventilation rates and indoor air quality (IAQ). Hence, in this work we aimed to investigate the influence of ventilation rates on IAQ for an indoor ventilated enclosure. Herein, ventilation efficiency is represented by the maximal local volume-averaged concentration and recirculation rate. In the present study, computation fluid dynamics (CFD) was applied and the low-Re-number $k-\varepsilon$ model (verified by experiments) was selected for Reynolds-averaged Navier–Stokes (RANS) simulations, with buoyancy effects considered due to density differences. We found that when increasing the inlet ventilation rates, the impact on indoor pollutant concentration was considerable due to the increase in the turbulent diffusion effects. Moreover, this was less dependent on the larger range of slot Reynolds numbers (for the current study, $Re_s \geq 3000$) and it ultimately tends to show an asymptotic behavior, which refutes the common working hypothesis of "the larger the ventilation rates, the better the IAQ". These findings should further play an important role in the design of energy-efficient ventilation systems.

1 Introduction

The essential function of building ventilation systems is to supply fresh air and to remove contaminants, thereby providing a healthy and comfortable environment within the building. Many studies have investigated the relationship between inadequate ventilation in buildings and human responses,[1–4] which could involve various health-related effects (*i.e.*, SBS—sick building syndrome). It is well recognized that the energy consumption involved in building ventilation usually represents a significant portion (30–60%) of the total energy use of a building's facilities,[5] along with substantially contributing to CO_2 emissions.[6] Hence in terms of economics and the environment, the design of a high-quality and energy-efficient ventilation strategy for building systems is of considerable interest.

Nowadays, the design of building ventilation systems is mainly based on experience and the rule of thumb, and a large safety margin is applied for the ventilation rate. This often results in excessive ventilation for the building ventilation design in question, causing an unnecessary additional energy cost. Current codes and standards do not offer adequate guidance with respect to energy efficiency, or for the relationship between the ventilation rate and the degree of indoor hazard. This motivates researchers to study (either *via* experimental monitoring or numerical simulations) the influence of ventilation rates on contaminant removal efficiency for different building environments. Yi, Kim and Bae studied the effect of air flow rates on gas capture efficiency in a kitchen environment and finally recommended optimal supply rates.[7] Moschetti and Carlucci investigated the impact of design ventilation rates on indoor air quality in residential buildings.[8] Dutton and Fisk evaluated the energy (multiple ventilation rates) and indoor air quality (indicated as formaldehyde concentration) implications of various fixed minimum ventilation rates.[9] By integrating building simulation and CFD methods, Fan and Ito found an appropriate air flow pattern was required for contributing to creating a healthy environment as well as for making energy savings.[10] From these studies, they agreed that indoor air flow characteristics play an important role in controlling contaminant removal, which was a point also discussed by other researchers.[11–16] Sepppanen and Fisk investigated the human responses to ventilation rates,[17] which is analogous to investigating the associated relationship between the contaminant concentration and ventilation rates as the rate of sick leave by employees is often dependent on the change in indoor contaminant concentration. From the existing studies, they summarized and demonstrated the predicted trends in illness of people who take sick leave *vs.* ventilation rates and

Department of Civil and Environmental Engineering, School of Urban Rail Transportation, Soochow University, No. 8 Jixue Road, Xiangcheng District, 215131, Suzhou, China. E-mail: shijie.cao@suda.edu.cn; donghao.zhu2014@gmail.com; Yyb8899@163.com; Fax: +86-512-67601052; Tel: +86-512-67501742

reported that the illness of sick leave decreases over time, but the decrease in rate varies dramatically for low ventilation rates. They also showed that with higher ventilation rates, the rate of sick leave decrease becomes negligible, tending toward an asymptotic behavior. Thus, the trends for the rate of contaminant concentration variation (decrease) will also show an asymptotic behavior. Furthermore, it was suggested that lower ventilation rates should be applied while maintaining optimal IAQ as a design-trend for ventilation systems. Different from those studies that are mostly focused on specific building environments, we aimed to investigate the effects of lower ventilation rates on indoor pollutant distribution based on the general transport routines of both airflows and pollutants, and further targeted the optimal ventilation rates, *i.e.*, the magnitude when the indoor concentration starts to show an asymptotic behavior. This method can be applied for other indoor environments. Since the Reynolds number is defined as the product of the supply velocity, the inlet-slot height, and the inverse of the kinematic viscosity, lower ventilation rates can be straightforwardly linked to different transitional inlet-slot Reynolds numbers, which is a main focus in the current work.

Moreover, two points should be emphasized in our work: first, the transitional flow effects on pollutant distribution were investigated, where these are due to the lower rates based upon typical ventilation requirements from ACH (air change rates), *i.e.*, 4–15;[18] second, the ventilation efficiency is newly defined and represented by the magnitudes of the maximal volume-averaged indoor contaminant concentration and the maximal mass flow recirculation rates. With these low Reynolds numbers, several potential hypotheses of "airflows and pollutants" inspired this research: transitional effects near the inlet should be noted and may play an important role in the pollutant removal process, as they impact on the local transition to turbulence of the inlet air-jet; in addition, when the inlet-slot Reynolds number (supplied ventilation rates) exceeds a certain level (or magnitude), the indoor pollutant concentration will cease to decrease and will tend toward an asymptotic behavior; indoor ventilation rates should be provided based on the actual distribution of the pollutant source rather than on simple ACH values.

Numerical simulations or small-scale experiments are usually employed to assure highly efficient and well-performing ventilation systems.[19–21] Therefore, numerical simulation with CFD methods was a main tool utilized in the current work. A low-Re-number k–ε model was applied for the numerical simulations of a simple ventilation benchmark case (with a typical size of classroom). A range of transitional slot Reynolds numbers $\mathrm{Re_s}$ at the inlet were selected (ranging from 790 to 4000), corresponding to the low velocities typically required for ventilation comfort in full-scale applications. In the simulations, a surface pollutant source (*i.e.*, CO_2 as a indicator, as a common indoor pollutant) was also included for evenly distributed pollutant sources, allowing us to look at predicted pollutant concentrations.

The present manuscript is further structured as follows. First, in Section 2, the governing equations used in the simulations are briefly reviewed. Next, the details of the numerical setup are described in Section 3. Subsequently, Section 4 presents a number of Reynolds-averaged Navier–Stokes (RANS) simulations, in which the effects of inlet boundary conditions of the slot Reynolds numbers on ventilation efficiency are evaluated. Finally, the conclusions are presented in Section 5.

2 Governing equations for indoor ventilation

2.1 Governing equations

In the present study, a simple benchmark ventilation case is considered for an indoor environment (size based on a typical class room) consisting of an inlet and outlet as well as a source distribution of gaseous pollutants S_p (see Fig. 1 for a sketch), with the volume of the room Ω, and inlet-vent area A. The room conditions are isothermal (*i.e.*, the supplied air temperature remains the same as the indoor one with at 288 K, and steady state). Two species are considered in this work, *i.e.*, air and CO_2 (considered as a typical indoor pollutant), with the mass fraction, respectively, corresponding to $1 - Y$ and Y. Clean air for ventilation is supplied with an average velocity U_0, and a density ρ_0 at the inlet.

The normalized transport equations are applied in this system. A particular normalization is selected, *i.e.*, the reference length $L = \Omega^{1/3}$, where the reference velocity is U_0, and the reference density corresponds to ρ_0. For the concentration, the well-mixed pollutant concentration (the average mass fraction) Y_0 at the ventilation outlet is used as a reference. The mass-flux

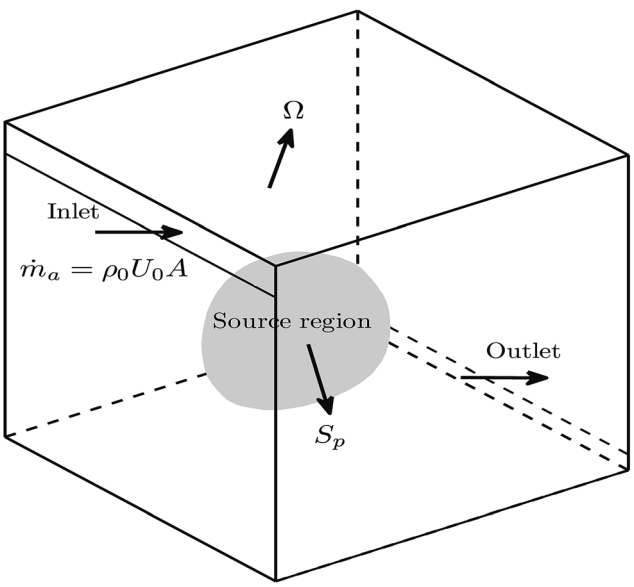

Fig. 1 Outline of a simple indoor ventilation case.

Table 1 Summary of the terms and expression used in the RANS equations

$\dot{m}_\mathrm{a} = \rho_0 U_0 A,\ \dot{m}_\mathrm{p} = \iiint_\Omega S_\mathrm{p}(x)\mathrm{d}x,\ Y_0 = \dot{m}_\mathrm{p}/(\dot{m}_\mathrm{a} + \dot{m}_\mathrm{p}) = 1/(1+\alpha)$
$S^*_\mathrm{p} = S_\mathrm{p} L^3/\dot{m}_\mathrm{p},\ \nu_0 = \mu_0/\rho_0,\ D_t = \nu_t/\mathrm{Sc}_t$

Table 2 Constants and damping functions used in the turbulence model

$[\mathrm{Sc}_t, C_\mu, C_1, C_2, C_3, \sigma_k, \sigma_\varepsilon] = [0.9, 0.09, 1.44, 1.44, 1.92, 1.0, 1.3]$
$f_\mu = [1.0 - \exp(-0.0215\mathrm{Re}_k)]^2(1 + 31.66/\mathrm{Re}_t^{5/4}), f_1 = f_3 = 1.0$
$f_2 = [1.0 - 0.01\exp(-\mathrm{Re}_t^2)][1 - \exp(-0.0613\mathrm{Re}_k)],$
$\mathrm{Re}_k = \sqrt{k}y/\nu,\ \ \mathrm{Re}_t = k^2/\nu\varepsilon$

of air into the domain corresponds to $\dot{m}_a$, while the mass-flux of the pollutant corresponds to $\dot{m}_p$, such that $Y_0 = \dot{m}_p/(\dot{m}_a + \dot{m}_p) = 1/(1 + \alpha)$, with $\alpha \equiv \dot{m}_a/\dot{m}_p$. Using this normalization, the non-dimensional RANS equations, using an eddy viscosity and eddy diffusivity to model the Reynolds stresses and fluxes, respectively, are given by Cao and Meyers.[22] When the ratio α is sufficiently large ($\alpha \to \infty$), the flow equations can be decoupled from the pollutant concentration equation, although flow equations can be decoupled only if α is bigger than 10^5 when CO_2 is considered as the pollutant species.[23] Now, we briefly summarize the resulting normalized RANS equations for the continuity, momentum, and concentration equations, respectively, corresponding to:

$$\nabla^*\cdot\left(\bar{\rho}^*\tilde{\mathbf{u}}^*\right) = \frac{K}{\alpha}S_p^*, \tag{1}$$

$$\nabla^*\cdot\left(\bar{\rho}^*\tilde{\mathbf{u}}^*\otimes\tilde{\mathbf{u}}^*\right) + \nabla^*\bar{p}^* - \frac{2}{\mathrm{Re}}\nabla^*\cdot\left(1+\nu_t^*\right)[S^* - tr(S^*)I/3] - \mathrm{Ri}\frac{\tilde{C}^*}{1+\alpha}\ \frac{\bar{\rho}^*}{\rho_p^*} = 0, \tag{2}$$

$$\nabla^*\cdot\left(\bar{\rho}^*\tilde{\mathbf{u}}^*\tilde{\boldsymbol{C}}^*\right) - \frac{1}{\mathrm{Re}\times\mathrm{Sc}}\nabla^*\cdot\left(1+D_t^*\right)\nabla^*\tilde{\boldsymbol{C}}^* = \left(1+\frac{1}{\alpha}\right)KS_p^*, \tag{3}$$

where, $\tilde{\mathbf{u}}^*$ and $\tilde{\boldsymbol{C}}^*$ are the time-averaged velocity and concentration; ν_t^* and D_t^* are the non-dimensional eddy viscosity and eddy diffusivity, defined as $\nu_t^* = \nu_t/\nu_0$, $D_t^* = D_t/D_0$ respectively; where ν_0 is the viscosity of air and D_0 is the mass diffusion coefficient; K is a constant ($K = A/L^2$, with A the area of the inlet-vent); S_p^* represents the non-dimensional pollutant source, and $S^* = [\nabla^*\tilde{\mathbf{u}}^* + (\nabla^*\tilde{\mathbf{u}}^*)^T]/2$ is the strain rate tensor. Furthermore, the non-dimensional parameters in eqn (1) and (2) are the Reynolds number (Re), Schmidt number (Sc), and Richardson number (Ri):

$$\mathrm{Re} = \frac{U_0L}{\nu_0},\ \ \mathrm{Sc} = \frac{\nu_0}{D},\ \ \mathrm{Ri} = \frac{g(\rho_p - \rho_0)L}{\rho_0 U_0{}^2}. \tag{4}$$

More details and definitions can be found in Table 1. By looking at the non-dimensional forms of the continuity and concentration equations (eqn (1) and (3)), it is found for $\alpha \to \infty$ that:

$$\lim_{\alpha\to\infty}\left[\frac{K}{\alpha}S_p^*\right] = 0;\ \ \lim_{\alpha\to\infty}\left[\mathrm{Ri}\frac{\tilde{\boldsymbol{C}}^*}{1+\alpha}\frac{\rho^*}{\rho_p^*}\right] = 0;\ \ \lim_{\alpha\to\infty}\left[\left(1+\frac{1}{\alpha}\right)KS_p^*\right] = KS_p^*. \tag{5}$$

Hence, for $\alpha \to \infty$, the solution of the continuity and momentum balance are decoupled from the pollutant concentration $\tilde{\boldsymbol{C}}^*$. Consequently, the pollutant transport equation of $\tilde{\boldsymbol{C}}^*$ becomes a linear-partial-differential equation (concentration will become a passive scalar), which can be solved once the velocity field is known (*e.g.*, based on a set of numerical simulations or experiments).

In the current work, we do not treat concentration as a passive scalar based on the relative α range investigation (calculated from the air change rates); therefore, the presence of buoyancy effects caused by density differences is also considered in the momentum equations.

2.2 Turbulence modeling

Due to the influence of the buoyancy effects, the k–ε models are modified, which are employed to close the Navier–Stokes equations, accompanied with buoyancy source terms in the turbulent transport equations for both the turbulent kinetic energy k and turbulent dissipation ε.[24–27] Further, k and ε are still described under the steady state shown below:

$$\nabla^*\cdot\left(\bar{\rho}^*\tilde{\mathbf{u}}^*\otimes k\right) = \frac{1}{\mathrm{Re}}\nabla^*\cdot\left(\nu + \frac{\nu_t}{\sigma_k}\right)\nabla^*k + P_k^* - \varepsilon + G_k^*, \tag{6}$$

$$\nabla^*\cdot\left(\bar{\rho}^*\tilde{\mathbf{u}}^*\otimes\varepsilon\right) = \frac{1}{\mathrm{Re}}\nabla^*\cdot\left(\nu + \frac{\nu_t}{\sigma_\varepsilon}\right)\nabla^*\varepsilon + \frac{\varepsilon}{k}\left(C_1f_1P_k^* - C_2f_2\varepsilon + C_3f_3\max\left(0, G_k^*\right)\right). \tag{7}$$

where P_k^* is the turbulent production term, modeled as $P_k^* = \nu_t\nabla^*\tilde{\mathbf{u}}^* : \nabla^*\tilde{\mathbf{u}}^*$ and G_k^* is the production of k due to buoyancy effects and is based on the eddy diffusivity model:

$$G_k^* = -\mathrm{Ri}\frac{1}{1+\alpha}\frac{1}{\rho_p^*}\overline{\rho^*u^{*\prime\prime}C^{*\prime\prime}} = -D_t^*\mathrm{Ri}\frac{1}{1+\alpha}\frac{1}{\rho_p^*}\nabla^*\tilde{\boldsymbol{C}}^* \tag{8}$$

Finally, the additional constants Sc_t, C_μ, C_1, C_2, C_3, σ_k, σ_ε, and functions f_μ, f_1 and f_2 are defined in Table 2.

3 Numerical setup of the benchmark casez

In the current study, a series of RANS simulations are performed for the same ventilated enclosure, consisting of the ventilated enclosure in which we located the inlet boundary condition at the inlet slot of the room (*cf.* Fig. 2 for details of the geometry and grid). This simplified geometry was modulated as a small classroom with six students (with a classroom size of 5 m × 4 m × 3.2 m). The CO_2 concentration and odor intensity were the dominant pollutants when considering the air supply rates. Generally, CO_2 is taken as the indicator for classrooms.[28] The generation rate of pollutant production of CO_2 from the students in our model was 4.5×10^{-6} m^3 s^{-1} (per person under sedentary status). A surface pollutant source was applied to represent the evenly distributed pollutant sources (*i.e.*, 6 students), *cf.* Fig. 3.

At the ventilation inlet, a uniform velocity U_0 was supplied, with a corresponding slot Reynolds number Re_s (defined using

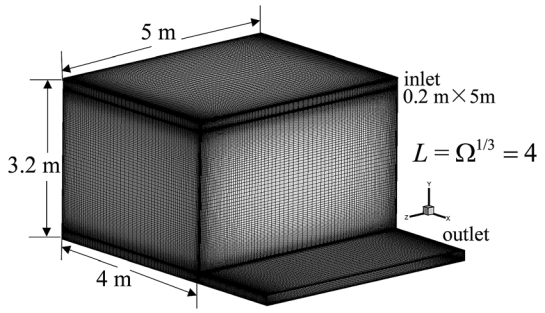

Fig. 2 Computational setup of the indoor ventilation benchmark case.

U_0, and the inlet-slot height of $0.05L$, 0.2 m) and Re (as defined in eqn (4), and Re is generally larger than Re_s, for the current case 20 times that of Re_s). Besides this, the turbulence intensity and non-dimensional turbulent length scale were, respectively, 5% and 0.01273 for the inlet boundary condition to define the turbulence levels, where the turbulent length scale corresponds to 7% of the hydraulic diameter of the supplied inlet and is often correlated to the value for fully-developed pipe flows or channel flows.[29] The turbulent intensities of the ventilation inlet are generally taken within the range 4–37%.[30]

The computational mesh was divided into a block-structure (*cf.* Fig. 2 containing a total of 2 256 784 cells (*i.e.*, $74 \times 195 \times 137$ for the main block)). The first grid-node of the mesh was typically positioned at a distance of $0.5 \times 10^{-3}L$ from the wall. For the current case, with a range of transitional Reynolds numbers, we verified that this ensures a distance from the wall, using inner units, that would remain well below $y^+ = 3$, so that the equations near the wall region could be sufficiently resolved to justify the application of the low-Reynolds-number k–ε model. A grid refinement study was also carried out with a finer grid using a total of 3 969 240 cells (compared to 2 256 784 for the baseline case). We found that the baseline case was sufficiently resolved, with differences in the velocity and turbulent kinetic energy between the two grid cases remaining below 2% (results are not shown here).

Table 3 Overview of the RANS simulation cases

ACH	U_0 (m s^{-1})	Re_s	Re	α	Ri
4	0.07	649	12 976	3226	14 978
5	0.09	811	16 220	4033	9586
6	0.11	973	19 465	4840	6657
7	0.12	1135	22 709	5646	4891
8	0.14	1298	25 953	6453	3745
9	0.16	1460	29 197	7259	2959
10	0.18	1622	32 441	8066	2397
11	0.20	1784	35 685	8872	1981
12	0.21	1946	38 929	9679	1664
13	0.23	2109	42 173	10 486	1418
14	0.25	2271	45 417	11 292	1223
15	0.27	2433	48 661	12 099	1065
16	0.28	2595	51 906	12 905	936
17	0.30	2757	55 150	13 712	829
18	0.32	2920	58 394	14 519	740
19	0.34	3082	61 638	15 325	664
20	0.36	3244	64 882	16 132	599

In order to study the impact of the slot Reynolds numbers Re_s on the effective ventilation efficiency, we also considered the dispersion of pollutants in the simulations. To this end, a case with a surface source of pollutants (*i.e.*, CO_2) inside the ventilated enclosure was considered, as shown in Fig. 3. For the sake of simplicity, the source was selected to be uniformly distributed over this surface. In the present work, the pollutant concentration will be dependent on the flow field and both are solved as a pair. Classrooms are environments generally with a high occupant density, which leads to a higher CO_2 concentration. The suggested ACH range for classrooms is 6–20 (ref. 31) In Table 3, a summary of the considered cases is provided, with different values for the Air Change per Hour, ACH, inlet velocities, U_0, slot Reynolds numbers, Re_s, Reynolds numbers, Re, mass-flux ratio, α, and Richardson numbers, Ri.

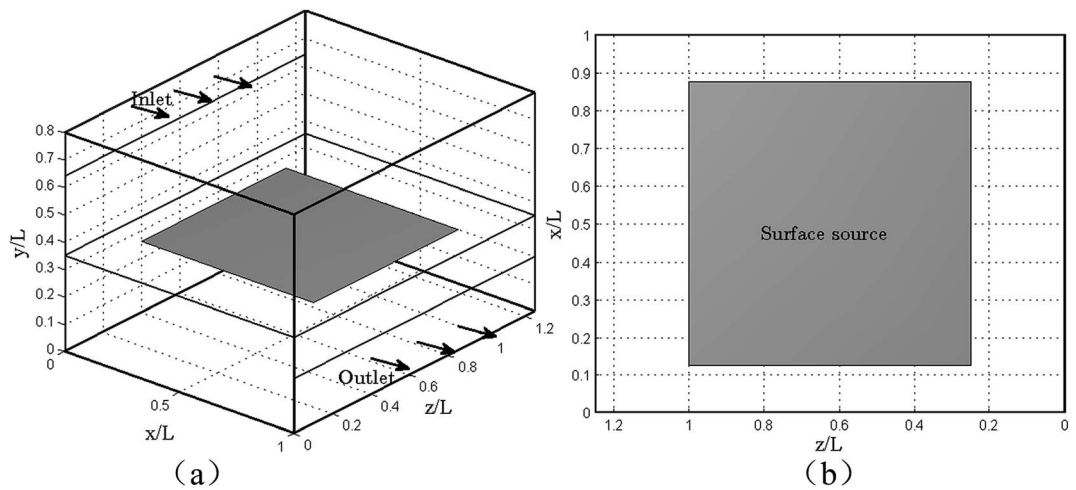

Fig. 3 Schematic view of a uniformly distributed pollutant surface source, located at the plane with a height of $y = 0.375L$ [(a) side view; (b) top view].

All the simulations were performed with the commercial software ANSYS Fluent. An incompressible pressure-based segregated solver was selected, using the SIMPLE algorithm and a second-order upwind scheme as used for the convective terms. The solutions were iteratively converged until the sum of the absolute normalized residuals of all the cells in the simulation domain remained below an upper threshold of 10^{-5} for the different equations. The temperature and dynamic viscosity, respectively, corresponded to 288 K and 1.7894×10^{-5} Pa s. The range of inlet ventilation rates were supplied in the range 0.07–0.36 m s^{-1}, providing smaller indoor rates within the required standard of 0.3 m s^{-1}.[18]

4 Results and discussion

In the current section, the impact of the inlet-slot Reynolds numbers on the predicted indoor ventilation is studied. We focus on cases with a range of transitional slot Reynolds numbers, *i.e.*, 649–3244, based on ACH ranging from 4–20. In Section 4.1, a comparison of the flow predictions is presented. Subsequently, in Section 4.2, we concentrate on internal turbulence levels and pollutant dispersion predictions for the different cases. Finally, aspects related to the ventilation efficiency are discussed in Section 4.3.

The low-Reynolds-number k–ε model of Chang, Hsieh, and Chen was employed for turbulence modeling,[32] which has already proved to be a suitable RANS model for indoor ventilation simulation with transitional slot Reynolds numbers.[30,31] Flow predictions with different RANS turbulence models were compared with previous PIV experimental data reported by Twan van Hooff and Bert Blocken[33] Further, this model can overcome substantial modeling errors at the inlet geometry of our setup compared to other turbulence RANS models, such as the RNG k–ε model. In Fig. 4, both simulations and experiments were performed for the same Reynolds number $\mathrm{Re_s} = 5400$ (within the transitional flow range) and geometry. This showed that both the simulations and experiments were in good agreement.

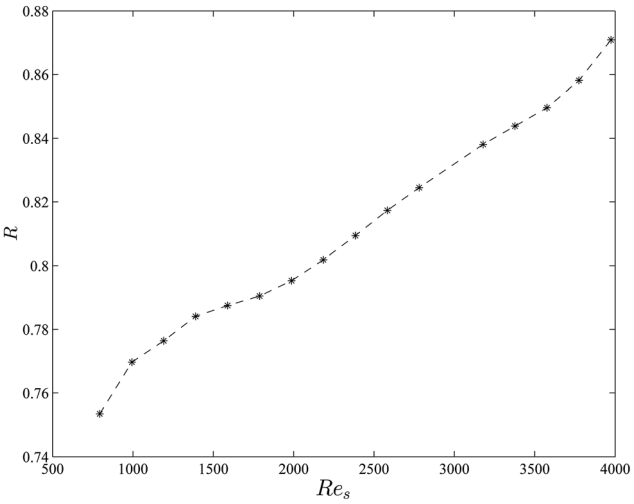

Fig. 5 Dependence of the recirculation R with respect to different inlet-slot Reynolds numbers using the low-Re-number k–ε model.

4.1 The influence of slot Reynolds numbers on velocity field

In the current section, we investigate the effect of inlet-slot Reynolds numbers on velocity, keeping the turbulent intensity constant at a level of 5%. We considered the indoor environment, *cf.* Fig. 2, consisting of an inlet and an outlet, but extended with a pollutant source on a horizontal surface at a height of $y = 0.375L$ (*cf.* Fig. 3 for detail).

In order to evaluate the flow field, the recirculation rate R was applied, which determines the maximum back mass flow relative to the total mass flow, representing the ventilation efficiency to some extent, as was defined in Cao and Meyers:[22]

$$R = \max_{0<x<L}\left[\frac{\iint_{\Omega_x} \max[-\rho \mathbf{u}\cdot\mathbf{e}_1, 0]\mathrm{d}\Omega}{\iint_{\Omega_x} \rho \mathbf{u}\cdot\mathbf{e}_1 \mathrm{d}\Omega}\right], \quad (9)$$

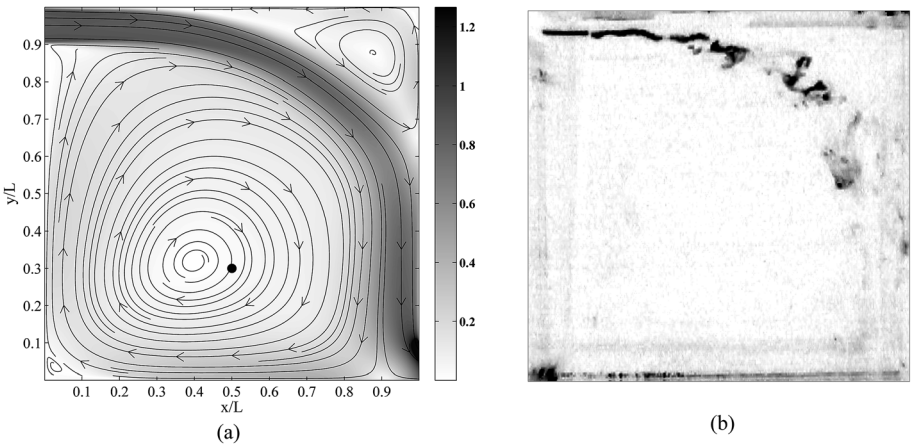

Fig. 4 Contours of dimensionless air flow velocity, and pollutant concentration at xy-plane ($z = 0.5L$). (a) Velocity field from RANS simulation; (b) corresponding flow visualization from experiment.

where $\mathbf{e}_1$ is the unit vector in the x-direction and Ω_x is a surface perpendicular to the x-direction, at location x, $0 \leq R \leq \infty$.

Fig. 5 shows that the recirculation rate increases with the increase of the inlet-slot Reynolds numbers, which will help to improve the indoor pollutant removal efficiency. Fig. 6 demonstrates the streamlines and the magnitude of the velocity, the turbulent viscosity, and the concentration for three different inlet-slot Reynolds numbers. We only took three different slot Reynolds numbers (*i.e.*, $Re_s = 1135$, $Re_s = 2433$, $Re_s = 3244$) for the representation of the slot Reynolds numbers, corresponding to the values given in Table 3. When looking at the results in Fig. 6(a1–a3), it can be seen that the effect of the inlet-slot Reynolds numbers on the velocity is not trivial. With increasing inlet-slot Reynolds numbers, the separation point of the inlet-jet shifts upwards along the downstream, which changes the internal recirculation shape and magnitude.

4.2 Influence of the slot Reynolds numbers on turbulence and concentration field

In this section, we investigate the impact of the inlet-slot Reynolds numbers on indoor turbulence levels and pollutant concentration. For the same cases with three different slot Reynolds numbers (*i.e.*, $Re_s = 1135$, $Re_s = 2433$, $Re_s = 3244$), it was found that an increase in the slot Reynolds number at the inlet leads to an increased turbulent viscosity and eddy diffusivity in the ventilation domain, as shown in Fig. 6(b1–b3). Increases in the inlet-slot Reynolds numbers bring higher levels of turbulence in the jet region, which will further delay the inlet-jet separation along downstream. Finally, it will change the mass recirculation rate R (internal recirculation shape and magnitude), *cf.* Fig. 6. It can be remarked that the turbulence levels (turbulent viscosity) will affect eddy diffusivity; furthermore, they will influence indoor pollutant dispersion in indoor environments. The higher the turbulent viscosity is, the lower indoor pollutant concentration magnitude will be, as is shown in Fig. 6(c1–c3).

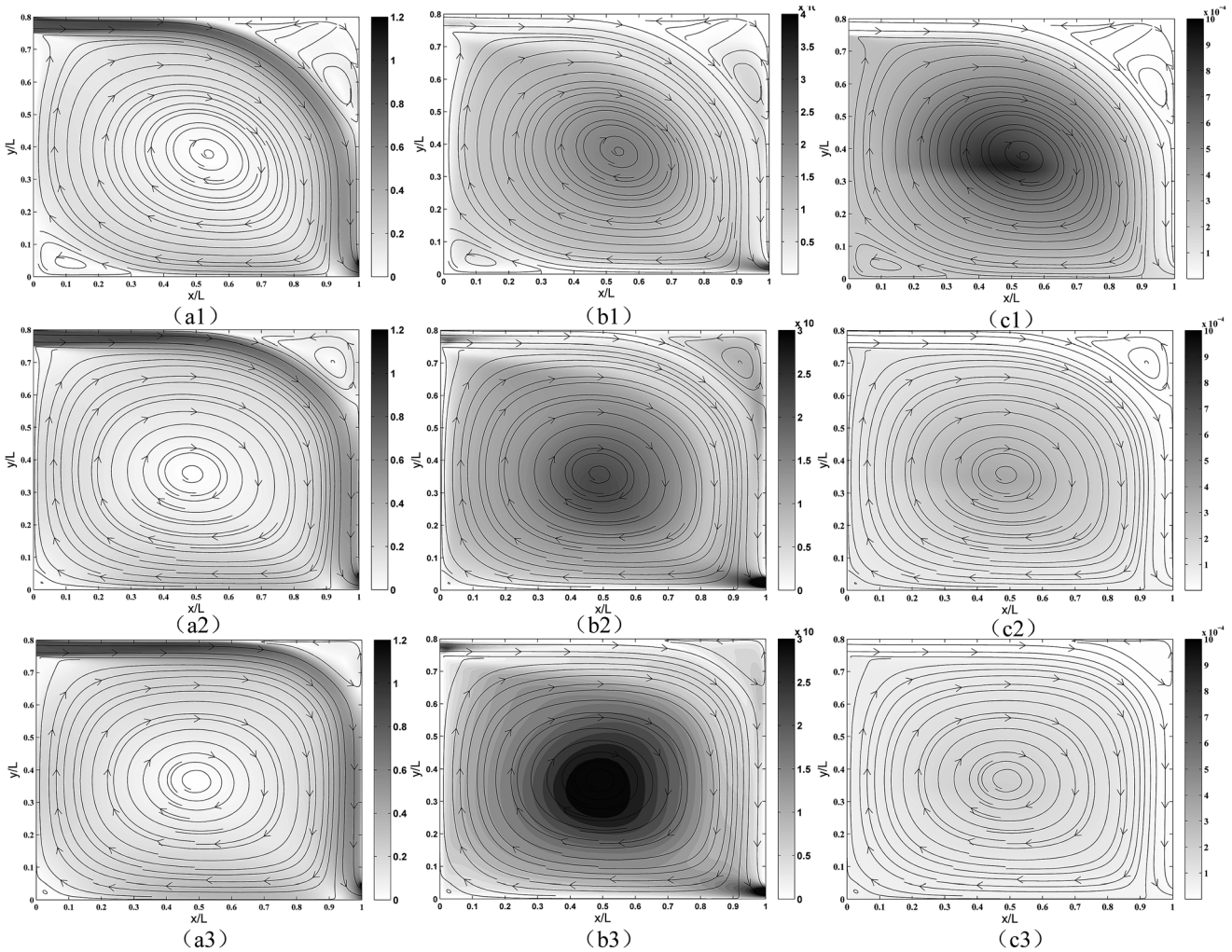

Fig. 6 Velocity, turbulent viscosity, concentration magnitude, and streamlines at the xy-plane ($z = 0.625L$) for different inlet-slot Reynolds numbers (Re_s) with the low-Re-number $k-\varepsilon$ model, respectively, corresponding to $Re_s = 1135$ (upper row), $Re_s = 2433$ (middle row), $Re_s = 3244$ (bottom row): [left column (a1–a3): velocity; middle column (b1–b3): turbulent viscosity; right column (c1–c3): concentration].

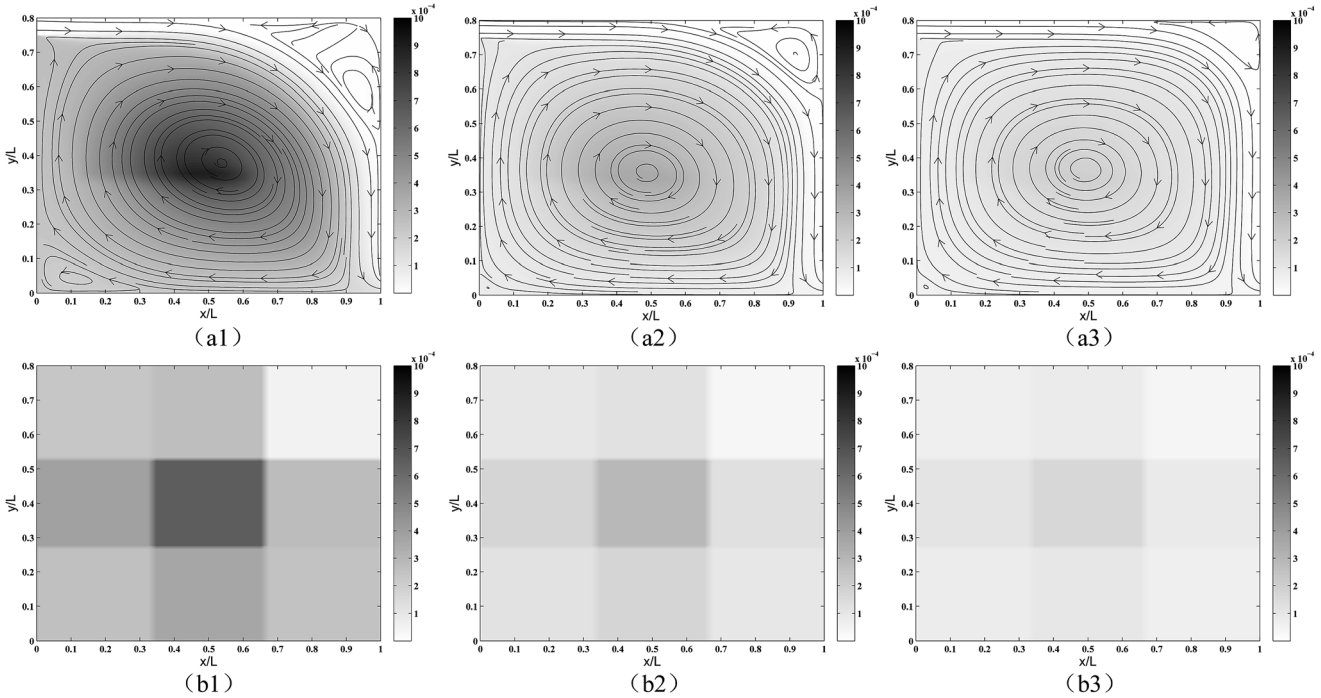

Fig. 7 Pollutant concentration distribution inside the ventilation enclosure, respectively, corresponding to $Re_s = 1135$ (left column, a1 and b1), $Re_s = 2433$ (middle column, a2 and b2), $Re_s = 3244$ (right column, a3 and b3): (a1–a3), using a high-dimensional representation (RANS), and (b1–b3) using a low-dimensional volume-averaging concentration, dividing the domain Ω into $3 \times 3 \times 3$ cubes Ω_c.

4.3 Influence of the slot Reynolds numbers on ventilation efficiency

In the last two sections, the influence of the inlet-slot Reynolds numbers on indoor flow and pollutant dispersion are presented. Specifically, they have a considerable impact on pollutant concentration distributions, as shown in Fig. 6(c1–c3). Now, we consider the locally averaged peak concentration $\langle \tilde{C}^* \rangle_{A,\max}$ representing the ventilation efficiency, as defined below:

$$\langle \tilde{C}^* \rangle_{A,\max} = \max\left(\frac{1}{\Omega_c} \iiint_{\Omega_c} \tilde{C}^*(x) \mathrm{d}x \right). \quad (10)$$

Since the peak concentration itself is mathematically not always meaningful (*e.g.*, pollutant point sources locally leading to infinite concentration levels), in this case, the concentration locally averaged over a volume of $(0.3L)^3$ was selected. Fig. 7 shows a comparison of the concentration distributions directly resulting from the RANS model and the low-dimensional concentration locally averaged over a volume of $(0.3L)^3$, with the corresponding slot Reynolds numbers Re_s equal to 1135, 2433, and 3244, respectively. It can be shown that the concentration distribution (Fig. 7(a1–a3)) of the pollutant is qualitatively reflected by the concentration locally averaged over a volume of $(0.3L)^3$, *cf.* Fig. 7(b1–b3). Moreover, the pollutant concentration magnitudes decreased as we increased the slot Reynolds numbers. Hence, the low-dimensional volume-averaged concentration can be utilized for indoor concentration distribution. Furthermore, this will facilitate the practical use in monitoring the pollutant dispersion.

We now quantify the effect of changing the inlet-slot Reynolds numbers on the indoor ventilation efficiency. Fig. 8 shows the evolution of the locally averaged peak concentration for the different simulations as a function of the slot Reynolds numbers at the inlet. In Fig. 7, it can be observed that the inlet-slot Reynolds numbers have a large impact on the pollutant concentration prediction, as already shown in Fig. 6(c1–c3), similar to previous findings.[34] It was also found that the variation of the peak concentration decreases as the slot Reynolds numbers increase and it becomes negligible when the slot Reynolds exceeds a certain level, *i.e.*, $Re_s = 3000$. Moreover, $Re_s = 3000$ corresponds to ACH = 15, which is also the maximal recommended air change per hour for general residential environments.[18] Since we only focused on transitional slot Reynolds numbers, it can be estimated that if the slot Reynolds numbers are sufficiently large, this peak concentration will tend to show an asymptotic behavior. This violates the common sense that the larger the inlet ventilation rates (larger slot Reynolds numbers), the better the indoor pollutant will be removed, resulting in a waste of building energy consumption.[5] Hereby, we need to point out that the asymptotic behavior is not necessarily restrained to the maximal local-averaged volume concentration but also exists for normal volume-averaging concentrations (results not shown here).

Our findings show similar behaviors to those shown in previous studies with experimental investigations.[9,17] However, it should be noted that our findings are only specific for

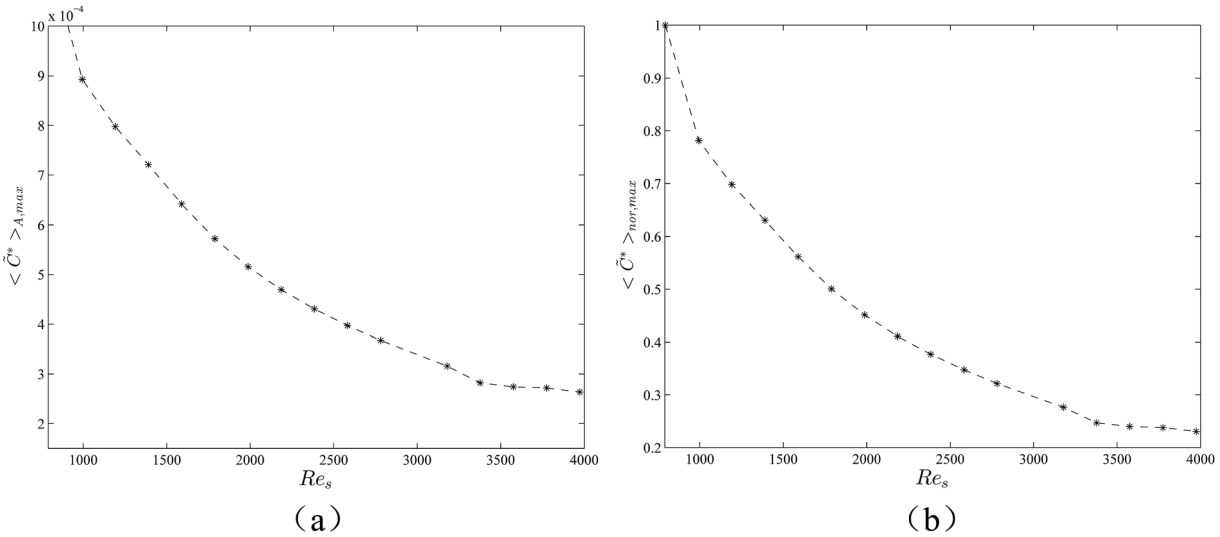

Fig. 8 Maximum of local-averaged concentrations (averaged over a local volume with size $(1/3L)^3$) as function of different inlet-slot Reynolds numbers using the low-Re-number k–ε model (a) (in (b), the values are relative to $Re_s = 649$).

ventilation cases with the current transitional slot Reynolds numbers, although the same idea could be extended to other complex building environments.

5 Conclusions

In the present study, we performed a series of RANS simulations to investigate the influences of inlet-slot Reynolds numbers on contaminant predictions and ventilation efficiency in indoor ventilation systems. A benchmark ventilation case was simulated based on an evaluation of the low-Re-number k–ε model of Chang—a suitable RANS model for ventilation simulation at transitional slot Reynolds numbers.

In practice, a common working hypothesis was that the larger the supplied ventilation rates, the better the indoor pollutant removal efficiency would be. Nowadays, trends in ventilation are moving toward lower ventilation rates while keeping the same optimal indoor environment. Hence, it is of great importance to study the ventilation cases with lower (transitional) inlet-slot Reynolds numbers (directly related with supplied ventilation rates), which was the main focus for the current study. We then evaluated the relationship between the inlet-slot Reynolds numbers and indoor ventilation efficiency, represented by the recirculation rate and maximal locally volume-averaged concentration. It was observed that inlet-slot Reynolds numbers have an important impact on indoor flow pattern, resulting in changing the shape and magnitude of internal recirculation, thus further influencing the contaminant dispersion. The results of the current work also indicated that the inlet-slot Reynolds numbers have a considerable effect on turbulence levels, *i.e.*, turbulent viscosity and eddy diffusivity, which also influence the indoor pollutant concentration distribution. The larger the inlet-slot Reynolds numbers, the smaller the pollutant concentration will become. Moreover, it was found that the pollutant concentration distribution is less dependent on the larger range of slot Reynolds numbers (for the current study, *i.e.* $Re_s \geq 3000$) and that the concentration ceases to tend to show an asymptotic behavior. Hence, this conclusion violates the common working hypothesis, *i.e.*, that the larger the supplied ventilation rates, the better the indoor pollutant removal efficiency will be. This further shows that it is of great importance to apply indoor pollutant on-line monitoring for the design of energy-efficient ventilation systems.

For the current study, we used the peak concentrations averaged over an observation volume to represent ventilation efficiency, which was a straightforward method and may be a lot more interesting for practical use. This corresponds to a local volume average, where the size of such a volume may depend on the toxicity of the pollutant, lung capacity of human beings, *etc.* For real-life applications, ventilation systems with more complex geometries (including diffusers) should be considered for future research. Moreover, for the design of energy-efficient ventilation systems, both IAQ and thermal comfort should be considered. Thus, several other aspects should be taken into account for future studies, *e.g.*, in the presence of heat sources, human factors, *etc.*, as these could also be important influential factors for pollutant dispersion.

Acknowledgements

The authors would like to acknowledge the financial support from both Natural Science Foundation of Jiangsu Province and China (Grant no. BK20150328 and 51508362).

References

1 H. S. Chu, H. C. Yu, K. W. Mui and L. T. Wong, Ventilation of general hospital wards for mitigating infection risks of three kinds of viruses including Middle East respiratory syndrome *Coronavirus*, *Indoor Built Environ.*, 2016, DOI: 1420326X16631596.

2 D. G. Shendell, R. Prill, W. J. Fisk, M. G. Apte, D. Blake and D. Faulkner, Associations between classroom CO_2 concentrations and student attendance in Washington and Idaho, *Indoor Air*, 2004, **14**, 333–341.
3 D. K. Milton, P. M. Glencross and M. D. Walters, Risk of Sick Leave Associated with Outdoor Air Supply Rate, Humidification, and Occupant Complaints, *Indoor Air*, 2000, **10**, 212–221.
4 J. Sundell, H. Levin, W. W. Nazaroff, W. S. Cain, W. J. Fisk, D. T. Grimsrud, F. Gyntelberg, Y. Li, A. K. Persily, A. C. Pickering, J. M. Samet, J. D. Spengler, S. T. Taylor and C. J. Weschler, Ventilation rates and health: multidisciplinary review of the scientific literature, *Indoor Air*, 2011, **21**, 191–204.
5 M. W. Liddament, Energy Conservation in Buildings and Community Systems Programme. Annex V Air Infiltration and Ventilation Centre, *A guide to energy efficient ventilation*, Air Infiltration and Ventilation Centre, 1996.
6 Z. T. Ai, C. M. Mak, D. J. Cui and P. Xue, Ventilation of air-conditioned residential buildings: a case study in Hong Kong, *Energ. Build.*, 2016, **127**, 116–127.
7 K. W. Yi, Y. Kim and G. N. Bae, Effect of airflow rates on concurrent supply and exhaust kitchen ventilation system, *Indoor Built Environ.*, 2016, **25**, 180–190.
8 R. Moschetti and S. Carlucci, The impact of design ventilation rates on the indoor air quality in residential buildings: an Italian case study, *Indoor Built Environ.*, 2016, DOI: 1420326X16643147.
9 S. M. Dutton and W. J. Fisk, Energy and indoor air quality implications of alternative minimum ventilation rates in California offices, *Build. Environ.*, 2014, **82**, 121–127.
10 Y. Fan and K. Ito, Integrated building energy computational fluid dynamics simulation for estimating the energy-saving effect of energy recovery ventilator with CO_2 demand-controlled ventilation system in office space, *Indoor Built Environ.*, 2014, **23**, 785–803.
11 Y. Cheng and Z. Lin, Experimental study of airflow characteristics of stratum ventilation in a multi-occupant room with comparison to mixing ventilation and displacement ventilation, *Indoor Air*, 2015, **25**, 662–671.
12 F. Li, E. S. Lee, J. Liu and Y. Zhu, Predicting self-pollution inside school buses using a CFD and multi-zone coupled model, *Atmos. Environ.*, 2015, **107**, 16–23.
13 T. Ai and C. M. Mak, Determination of single-sided ventilation rates in multistory buildings: evaluation of methods, *Energ. Build.*, 2014, **69**, 292–300.
14 Z. Zhang, W. Zhang, Z. Zhai and Q. Chen, Evaluation of various turbulence models in predicting airflow and turbulence in enclosed environments by CFD: Part 2-Comparison with experimental data from literature, *HVACR Res.*, 2007, **13**, 871–886.
15 Y. Cheng and Z. Lin, Technical feasibility of a stratum-ventilated room for multiple rows of occupants, *Build. Environ.*, 2015, **94**, 580.
16 A. Li and X. Wang, Airflow characteristics generated by fabric air dispersion ventilation, *Indoor Built Environ.*, 2015, **24**, 1059–1068.
17 O. A. Seppanen and W. J. Fisk, Summary of human responses to ventilation, *Indoor Air*, 2004, **14**, 102–118.
18 ASHRAE 62.2-2013, Standard 62.2-2013 – Ventilation and Acceptable Indoor Air Quality in Low-Rise Residential Buildings, 2013, ASHRAE 62.2-2013 Standard 62.2-2013 – Ventilation and Acceptable Indoor Air Quality in Low-Rise Residential Buildings.
19 Z. T. Ai and C. M. Mak, Large eddy simulation of wind-induced interunit dispersion around multistory buildings, *Indoor Air*, 2015, **26**, 259–273.
20 Y. Huang, Y. Wang, X. Ren, Y. Yang, J. Gao and Y. Zou, Ventilation guidelines for controlling smoke, dust, droplets and waste heat: four representative case studies in Chinese industrial buildings, *Energ. Build.*, 2016, **128**, 834–844.
21 N. Gao and J. Niu, CFD study on micro-environment around human body and personalized ventilation, *Build. Environ.*, 2004, **39**, 795–805.
22 S. J. Cao and J. Meyers, On the construction and use of linear low-dimensional ventilation models, *Indoor Air*, 2012, **22**, 427–441.
23 S. J. Cao and J. Meyers, Asymptotic requirements for the use of linear ventilation models in the presence of buoyancy forces, *Building Simulation*, 2014, **7**, 131–136.
24 W. Chung and C. B. Devaud, Buoyancy-corrected k–ε models and large eddy simulation applied to a large axisymmetric helium plume, *J. Numer. Methods Fluids*, 2008, **58**, 57–89.
25 L. Ricciardi, C. Prevost, L. Bouilloux and R. Sestier-Carlin, Experimental and numerical study of heavy gas dispersion in a ventilated room, *J. Hazard. Mater.*, 2008, **58**, 493–505.
26 J. Worthy, V. Sanderson and P. Rubini, Experimental and numerical study of heavy gas dispersion in a ventilated room, *Numer. Heat Transfer, Part B*, 2001, **39**, 151–165.
27 Z. Yan and G. Holmstedt, A two-equation turbulence model and its application to a buoyant diffusion flame, *Int. J. Heat Mass Transfer*, 1999, **42**, 1305–1315.
28 D. J. Clements-Croome, H. B. Awbi, Z. Bakó-Biró, N. Kochhar and M. Williams, Ventilation rates in schools, *Build. Environ.*, 2008, **43**, 362–367.
29 A. Dewan, *Tackling Turbulent Flows in Engineering*, Springer, New Delhi, 1st edn, 2011.
30 H. Awbi, *Ventilation of Buildings*, Taylor and Francis (E&FN Spon), London and NewYork, 2nd edn, 2003.
31 http://www.engineeringtoolbox.com/air-change-rate-room-d_867.html.
32 K. C. Chang, W. D. Hsieh and C. S. Chen, A modified low-Reynolds-number turbulence model applicable to recirculating flow in pipe expansion, *J. Fluids Eng.*, 1995, **117**, 417–423.
33 T. Van Hooff, B. Blocken and G. J. F. van Heijst, On the suitability of steady RANS CFD for forced mixing ventilation at transitional slot Reynolds numbers, *Indoor Air*, 2013, **23**, 236–249.
34 S. J. Cao and J. Meyers, Influence of turbulent boundary conditions on RANS simulations of pollutant dispersion in mechanically ventilated enclosures with transitional slot Reynolds number, *Build. Environ.*, 2013, **59**, 397–407.